Electron-density measurements in hohlraums using soft-x-ray deflectometry

C. D. Decker, R. A. London, J. A. Harte, L. V. Powers, and J. E. Trebes
Lawrence Livermore National Laboratory, Livermore, California 94550
(Received 10 September 1997)

This paper presents design calculations for experiments that measure electron densities of laser heated hohlraums with soft-x-ray moiré deflectometry. Hydrodynamical simulations of the hohlraums are analyzed to obtain deflection angles of the probing beam and x-ray emission from the hohlraum. The deflection angles and resulting moiré fringe shifts and fringe contrast are predicted to be sufficient to infer electron-density gradients from measurements. In addition, the self-emission is found to be much lower than that of the probing laser beam, giving a good signal-to-noise ratio. In conclusion, moiré deflectometry with soft-x-ray lasers has the potential to give valuable information about the electron density in laser driven hohlraums. [S1063-651X(98)06705-1]

PACS number(s): 52.70.La, 52.50.Jm, 52.25.Nr, 28.52.Av

I. INTRODUCTION

In the indirect drive laser fusion scheme [1], laser beams are focused onto the walls inside a high-Z hohlraum (see Fig. 1). The laser light is absorbed and converted into x rays that fill the hohlraum and implode a target capsule in the center via x-ray ablation. As the wall material is heated, it is ionized and expands into the hohlraum. This ''blowoff'' plasma can adversely affect the laser beam, the drive symmetry, and the capsule implosion in several ways. First, laser refraction and deposition in the blowoff plasma affect the x-ray-emission pattern. As the ablated plasma protrudes into the hohlraum interior, the region of laser deposition migrates away from the hohlraum wall along the beam path. Refraction from density gradients in the beam path can alter the propagation direction. These effects move the spatial location of peak x-ray production [2]. If the absorption length in the fill plasma becomes comparable to the laser path length, these effects can significantly modify the radiation pattern at the capsule and impair symmetry control. Second, absorption and scattering from plasma instabilities can both reduce the beam power and generate hot electrons that preheat the capsule, making it difficult to achieve high compression. Third, as the plasma blowoff stagnates on the axis, jets of plasma can disrupt the capsule implosion. One scheme to reduce wall blowoff is to fill the hohlraum with a low-Z gas that impedes the wall motion. However, the gas is readily ionized and forms a low-density plasma that can also degrade the hohlraum performance via refraction and plasma instabilities. In either case, detailed knowledge of the plasma density in the hohlraum is needed in order to understand and control these deleterious effects on the driving laser beam.

Current methods for measuring the plasma density in hohlraums include x-ray spectroscopy [3], incoherent x-ray imaging using backlighters, and absorption and scattering of the driving laser light [4]. Measurements using x-ray spectroscopy require detailed knowledge of the atomic processes occurring in the plasma in order to infer an electron density. Also, spectroscopic methods, such as Stark broadening, can only measure densities that are much higher than those expected in empty hohlraums. Imaging the hohlraum with an incoherent x-ray source is difficult because it is hard to produce an x-ray source brighter than the self-emission from the hohlraum. Measurements based on laser light absorption or scattering require a understanding of the nonlinear evolution and coupling of various parametric instabilities. Because of these difficulties, we consider a promising alternative.

One tool for measuring the electron densities in laser produced plasmas is the use of well-established Ne-like x-ray lasers [5]. Their high brightness and coherence enable a variety of probing schemes such as x-ray imaging, interferometry, and moiré deflectometry [6]. Although these techniques measure line integrated densities, they have the advantage of being a more direct measurement and do not require additional information such as the atomic state of the material under measurement.

A moiré pattern is created when light passes through two superimposed periodic structures. The ''beating'' of the periodic structures results in a coarse-grained moiré pattern. A commonly used periodic structure is a Ronchi ruling [6] consisting of opaque and transparent stripes of equal width and pitch. The moiré pattern of two rotationally offset Ronchi rulings is shown in Fig. 2(a). Lord Rayleigh [7] was the first to realize that a moiré pattern amplifies any small distortions in the periodic rulings and therefore can be used as a sensitive measurement tool.

One very useful application of the moiré effect is deflectometry, which measures angular deflections in a probe beam passing through the grids separated by some distance [see Fig. 2(b)]. The moiré pattern is formed by the projection

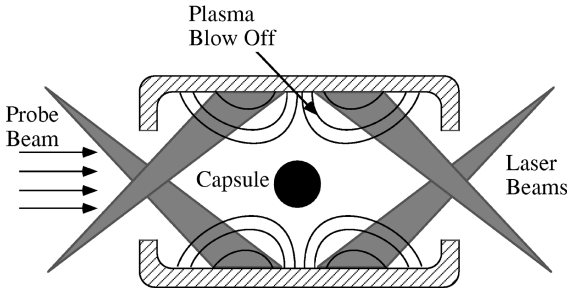

FIG. 1. Laser fusion hohlraum showing plasma blowoff from walls and x-ray probe beam.

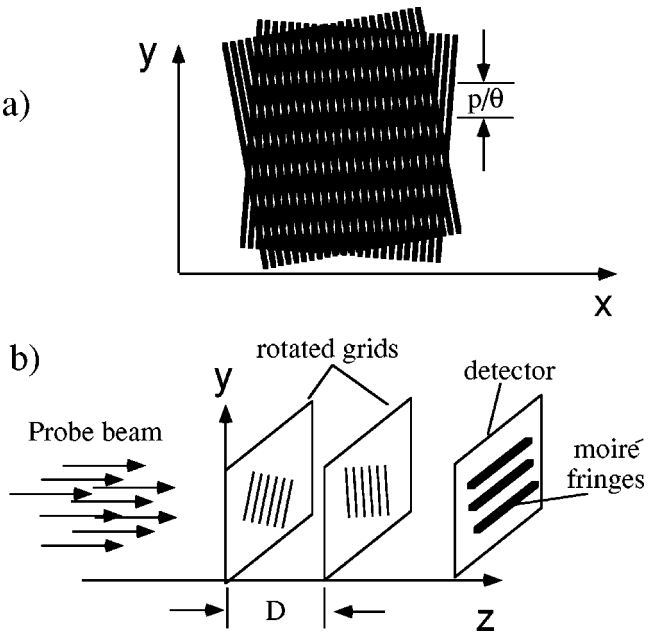

FIG. 2. (a) Moiré pattern formed by two rotationally offset Ronchi rulings. (b) Configuration for Moiré deflectometry showing the probe beam passing through two rotationally offset rulings separated by a distance D.

(shadow) of the first grid onto the second grid. Deflection of the probe beam distorts the shadow cast onto the second grid. Therefore, distortions in the moiré pattern can be used to measure angular deflections in the probe beam. Based on this effect, moiré metrology has been used extensively in a variety of applications such as characterization of optical components, strain analysis, study of fluid flow, and fluid mixtures [6]. Recently, electron-density measurements of laser heated exploding foils and plasma slabs have been made with moiré deflectometry [8]. As a result, an experimental effort has recently begun to measure electron densities in laser driven hohlraums [9] using a 155-Å Ne-like yttrium x-ray laser.

There are several key issues that must be addressed in order to ensure the success of these experiments. First, since hohlraums by themselves are very bright sources of x radiation [1], experiments must be designed to ensure that the probing x-ray laser produces a larger signal on the detector than does the background emission. Second, the diagnostic must be sensitive enough to measure the predicted densities. Third, the rapid temporal evolution of the plasma density may smear out the diagnostic. Predictions of this effect and calculations of the maximum x-ray laser pulse duration must be made.

In this paper we assess the feasibility of using moiré deflectometry to measure the electron densities in laser driven hohlraums. First we present a Fourier series analysis of moiré patterns and calculate the fringe spacing and fringe shifts as a function of deflection angle. Cylindrical geometry effects and data analysis are discussed. Next we present results of two-dimensional hydrodynamical simulations of hohlraums. From these simulations we obtain predicted electron-density profiles from which we calculate deflection angles and resulting moiré patterns. In addition, we calculate the background emission from the hohlraums and compare its brightness to that of the x-ray probe. Finally, data analysis methods are discussed.

II. MOIRÉ DEFLECTOMETRY

In this discussion we consider structures that are periodic in one dimension, i.e., Ronchi rulings. It is convenient to consider the transmission function $T(x,y)$ of such a grid, which can be represented in a Fourier series by

$$T(x,y)=\sum_n \left[a_n \cos\left(\frac{n\pi}{p}\{x+\delta x(x,y)\} \right) + b_n \sin\left(\frac{n\pi}{p}\{x+\delta x(x,y)\} \right) \right], \tag{1}$$

where the p denotes the spacing (pitch) of the rulings and $\delta x(x,y)$ denotes a perturbation in the rulings whose origin will be discussed below. Such a description can account for arbitrary line shapes and is useful when considering such things as fringe sharpening and fringe contrast [6]. However, in this discussion it will suffice to consider a much simpler grid such as a pure sinusoidal ($n=1$) grid. For such a grid rotated by an angle $\theta/2$ the transmission function T_1 is simply

$$T_1(x,y)=\frac{1}{2}\left[1+\sin\left(\frac{n\pi}{p}\{x\ \cos(\theta/2)-y\ \sin(\theta/2) + \delta x(x,y)\cos(\theta/2)\} \right) \right]. \tag{2}$$

Likewise, the transmission function T_2 of a second grid rotated by $-\theta/2$ is given by

$$T_2(x,y)=\frac{1}{2}\left[1+\sin\left(\frac{n\pi}{p}\{x\ \cos(\theta/2)+y\ \sin(\theta/2)\} \right) \right], \tag{3}$$

where we have assumed that the perturbation exists only on the first grid.

The resulting moiré pattern is given by the product of the two transmission functions

$$\begin{aligned} T_T(x,y)=T_1(x,y)T_2(x,y)=&\frac{1}{4}\sin\left(\frac{n\pi}{p}\{x\ \cos(\theta/2) - y\ \sin(\theta/2)+\delta x(x,y)\cos(\theta/2)\} \right) \\ &+\frac{1}{4}\sin\left(\frac{n\pi}{p}\{x\ \cos(\theta/2)+y\ \sin(\theta/2)\} \right) \\ &+\frac{1}{8}\cos\left(\frac{n\pi}{p}\{2x\ \cos(\theta/2)+\delta x(x,y)\cos(\theta/2)\} \right) \\ &+\frac{1}{8}\cos\left(\frac{n\pi}{p}\{2y\ \sin(\theta/2)+\delta x(x,y)\cos(\theta/2)\} \right). \end{aligned} \tag{4}$$

In the usual mode of operation, the high spatial frequencies of the Ronchi rulings are not resolved and the angle is

chosen small enough such that $\cos(\theta/2)\approx 1$, $2\sin(\theta/2)\approx\theta$. The last term on the right-hand side of Eq. (4) has the lowest spatial frequency and it represents the macroscopic moiré pattern. Therefore, concentrating on this term, we see that the moiré pattern consists of a transmission function of

$$T_M(x,y)=\cos\left(\frac{\pi}{p}\{2y\ \sin(\theta/2)+\delta x(x,y)\cos(\theta/2)\}\right). \tag{5}$$

Although Eq. (5) was derived for a sinusoidal grid structure, it contains most of the important features of the moiré pattern made by square grids. In the absence of the perturbations, the moiré pattern is just a set of equally spaced fringes periodic in the y direction with spacing Δ,

$$\Delta=\frac{p}{2\sin(\theta/2)}\approx\frac{p}{\theta}. \tag{6}$$

Before discussing the origin of the perturbation we mention a special case in which $2y\ \sin(\theta/2)\ll\delta x(x,y)$. In this so-called infinite fringe mode, the moiré fringes occur at $\delta x(x,y)=0,\pm p,\pm 2p,\ldots$. In this mode the moiré pattern forms a contour map of the perturbation.

For grids separated by a distance D, angular deflections $\delta\phi(x,y)$ of a collimated illuminating beam have the same effect as a ruling perturbation given by

$$\delta x(x,y)=D\,\delta\phi(x,y) \tag{7}$$

for $\delta\phi(x,y)\ll 1$. We emphasize that only angular deflections perpendicular to the first grid contribute to $\delta x(x,y)$. Angular deflections parallel to the first grid leave the projected image (shadow) invariant. Inserting Eq. (7) into Eq. (5), we find that the perturbation shifts the fringes by an amount $(D/\theta)\,\delta\phi$. Diffraction puts a restriction on the allowed values of the separation distance D. As collimated coherent light passes through the first grid it is diffracted and an interference pattern is formed. The interference pattern forms an exact replica of the object grid at integer multiples of the distance p^2/λ, where λ is the wavelength of the probing x-ray laser beam. This distance is known as the Talbot self-imaging plane. By placing the second grid at a Talbot plane, diffraction effects can be avoided. It is for this reason, as well as to avoid spatial smearing, that we must use collimated coherent laser light for moiré deflectometry.

When probe rays are propagated though a plasma with a density gradient they are deflected. Using the paraxial ray approximation, we find that the angular deflections perpendicular to the first grid are given by

$$\delta\phi=\frac{1}{2}\int_{-\infty}^{s_0}ds\,\frac{\nabla n_e}{n_c}\cdot\hat{x}, \tag{8}$$

where n_e is the electron density, n_c is the critical density for the probe beam, the integration is carried along the ray trajectory, and we have assumed $n_e\ll n_c$ to approximate the index of refraction of the plasma. By using Eqs. (5), (7), and (8) we can construct the resulting moiré pattern.

It is very instructive to consider a parabolic density profile of the form

$$n_e=n_0\left(1+\frac{r^2}{r_0^2}\right), \tag{9}$$

where r is the cylindrical radius of the hohlraum and n_0 and r_0 are constants. For this density profile we find

$$\nabla n_e\cdot\hat{x}=\frac{\partial n_e}{\partial r}\frac{x}{r}=\frac{2n_0x}{r_0^2}. \tag{10}$$

If the angular deflections are small we can approximate the ray paths with straight lines and the integration in Eq. (8) is trivial and we obtain $\delta\phi\approx(n_0/n_c)(xL_s/r_0^2)$, where L_s is the length of the ray path. The resulting moiré transmission function is found to be

$$T_M(x,y)=\cos\left(\frac{\pi}{p}\left\{y\theta+\frac{n_0}{n_c}\frac{DL_s}{r_0^2}x\right\}\right). \tag{11}$$

The moiré fringe pattern consists of a family of lines of constant phase $y\theta+(n_0/n_c)(DL_s/r_0^2)x=\text{const}$. These lines are parallel to each other and rotated by an angle $\sin^{-1}[(n_0/n_c)DL_s/\theta r_0^2]$ relative to the x axis. Although this result is strictly valid for a parabolic density profile, the rotated pattern is very common for cylindrical geometry, as we will show below.

III. HOHLRAUM SIMULATIONS

Predicting both the amount of angular deflection to the probing beam and the background emission requires detailed hohlraum simulations. Therefore, we performed two-dimensional (r,z) hydrodynamical simulations using the LASNEX code [10]. Details about hohlraum simulations with LASNEX can be found in Ref. [2]. The hohlraum and driving laser parameters are chosen to model typical experiments on the Nova laser facility at the Lawrence Livermore National Laboratory. In particular, we model an empty gold hohlraum with radius 0.8 mm and length 3.2 mm, driven by a 0.35-μm laser that rises in 100 ps to a peak power of 5.6 TW and stays flat for 1.0 ns before falling off in 100 ps. The pulse shape and power was chosen to model the ''foot'' of a standard Nova pulse. The laser entrance hole (LEH) has a radius of 0.6 mm giving a lip overhang of 0.2 mm.

We obtain from the simulation, among many other quantities, the electron density and temperature. In Fig. 3 we plot contours of the electron density for $t=0.6$, 0.8, 1.0, and 1.2 ns. At 0.6 ns the plasma from wall blowoff has just begun to protrude past the LEH. Since the soft-x-ray probe beam cannot penetrate the lip of the LEH it is fruitless to probe the hohlraum at earlier times. The shape of the plasma blowoff is indicative of the location of the driving laser beam spots. At 1.0 ns the blowoff from opposite sides of the hohlraum have met and stagnation has begun. We note that the electron temperature in the blowoff plasma remained around 2 keV during this time interval.

Having the electron density and temperature we can calculate the amount of self-emission coming from the hohlraum. To do this we postprocess the LASNEX data with a code [11] that solves the radiation transport equation for the specific intensity. To simulate a measured signal we integrate

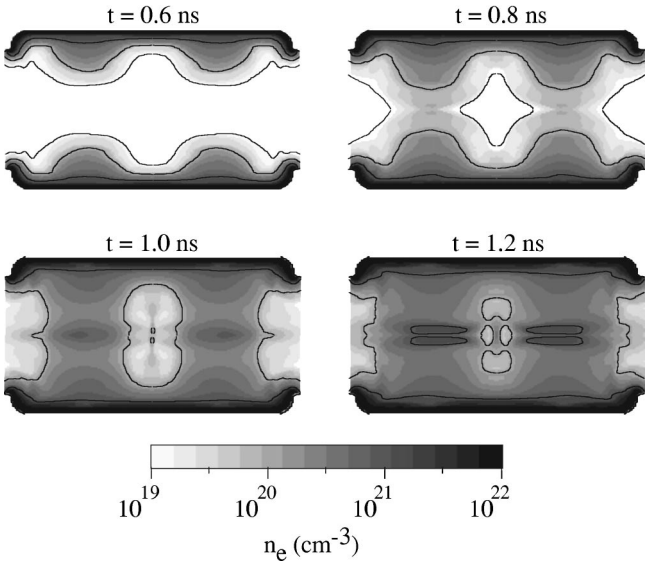

FIG. 3. Electron-density contours at several times. The contour levels are $n_e = 10^{19}$, 10^{20}, 10^{21}, and 10^{22} cm^{-3}.

the specific intensity over solid angle $\Delta\Omega$ and frequency bandwidth $\Delta h\nu$. The collimating optics determine the solid angle and various x-ray filters/mirrors determine the frequency window. We assume an experimental apparatus with $\Delta\Omega \sim 10^{-4}$ sr and $\triangle h\nu \sim 3$ eV. In Fig. 4 we plot both the self-emission and the x-ray laser signal as a function of the radius. Clearly the x-ray laser signal is significantly larger than that of the self-emission. We note, however, that the total (over all angles and frequencies) background emission greatly exceeds that of the x-ray laser. It is the collimated and narrow band properties (both contributing to brightness) that makes the x-ray laser such a useful diagnostic tool.

In the calculation of self-emission we have only considered continuum radiation from bremsstrahlung and bound-free transitions. However, it is possible that there exists line emission from atomic transitions that falls within the bandwidth of the detector. To ensure that line emission is not a problem we examined line positions and oscillator strengths for gold at the densities and temperatures predicted from the hydrodynamic simulations using an atomics structure code [12]. We found no strong lines within the frequency width of the detector.

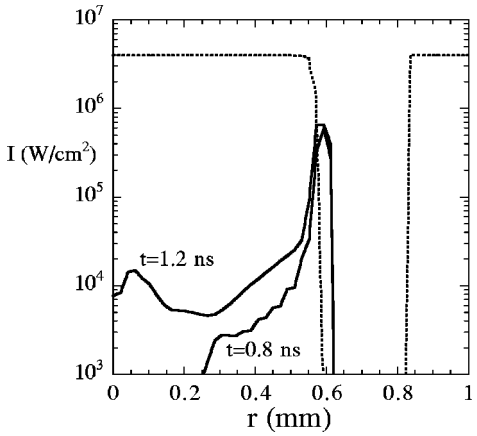

FIG. 4. Transmission of the x-ray laser (dashed line) and hohlraum self-emission (solid line).

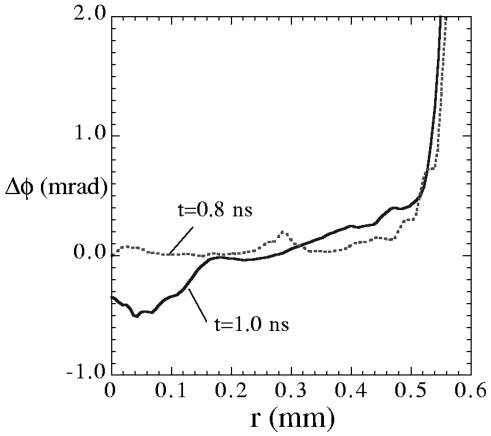

FIG. 5. Probing beam deflection angles versus radius for $t = 0.8$ (dashed line) and 1.0 ns (solid line).

Now we turn our attention to deflection angles, which are calculated using a ray tracing package in LASNEX which solves Eq. (8). In Fig. 5 we plot the deflection angles versus radius for $t = 0.8$ and 1.0 ns. The negative deflection angles on axis for the 1.0-ns case are from the stagnation points that refract the rays away from the axis.

Having obtained a distribution of deflection angles, we can then calculate the moiré pattern in the transverse x-y plane. It is at this point that we were able to design and evaluate this diagnostic. From Eqs. (6) and (7) it is apparent that we can regulate the background spacing and fringe shift by specifying the pitch p, rotation angle θ, and grid separation D. For simplicity, we kept the same values of p and θ as in previous experiments [8]. However, the grid separation was varied to obtain maximum sensitivity without producing moiré patterns that are too complicated to analyze. Using Eq. (5) we plot moiré patterns for $p = 10$ μm, $\theta = 2.5°$, and grid separation $D = 3.85$ cm (sixth Talbot plane) for $t = 0.6$, 0.8, 1.0, and 1.2 ns in Fig. 6. The fringe spacing $\Delta = 250$ μm. However, the hohlraum is imaged onto the moiré grids with an amplification factor of 4.5. Therefore, the fringe spacing

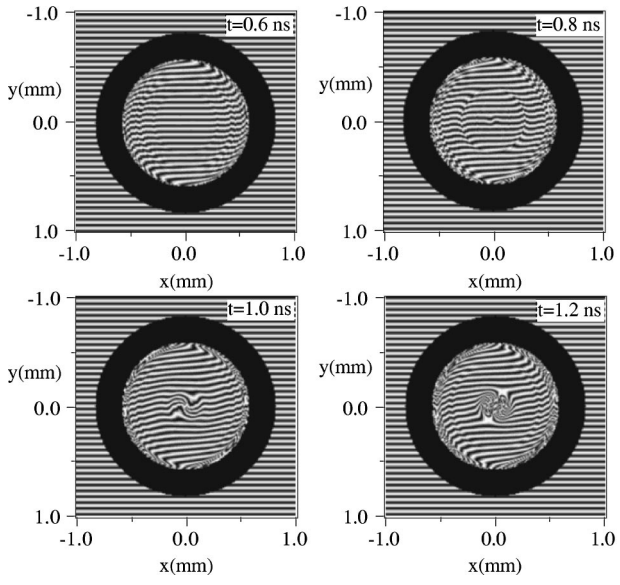

FIG. 6. Moiré patterns at several times.

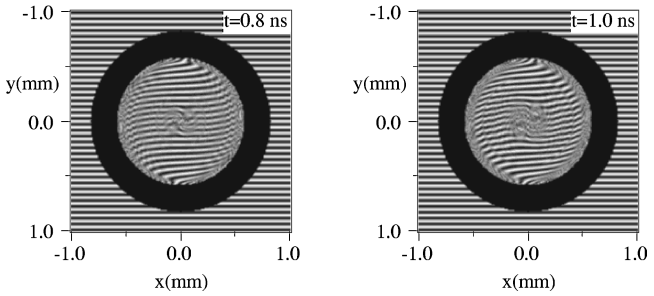

FIG. 7. Time-averaged Moiré patterns for an x-ray laser pulses of width 300 ps centered at 0.8 and 1.0 ns.

imaged back onto the hohlraum (object plane) is reduced to 56 μm. The spatial scales on Fig. 6 are for the object plane. The dark ring is due to the LEH lip. From Fig. 6 we see that at 0.6 ns there is slight fringe rotation from the plasma blowoff. At 1.0 ns the plasma has filled the hohlraum and results in a rotation of the fringe pattern. We note that at the latest time of 1.2 ns the stagnation has severely distorted the moiré pattern.

As shown in Fig. 3, there are rapid changes in the plasma density during the time in which we wish to probe (0.6–1.2 ns). These density changes cause rapid changes in the moiré pattern shown in Fig. 6. If the probing x-ray laser beam samples these changes the resulting moiré pattern will become smeared. To assess the amount of smearing we have temporally averaged the moiré patterns. In Fig. 7 we plot the temporally averaged moiré patterns for an expected x-ray laser pulse of 300 ps centered at 0.8 and 1.0 ns. Although there is some smearing, the resulting patterns have sufficient contrast to extract information about the density gradient, as we will show in the next section. We note that for x-ray pulse durations in excess of 500 ps the smearing is so great that little information can be gained. This clearly demonstrates the importance of using short-duration x-ray lasers for such measurements.

IV. DATA ANALYSIS METHODS

The actual moiré patterns obtained from hohlraum experiments can be very complicated, even in the absence of azimuthal variations to the electron density. Inferring the electron density from experimental images can be very difficult. As mentioned above, the moiré pattern is distorted by angular deflections perpendicular to the first grid and therefore only density gradients in one direction can be made, i.e., $\partial n_e/\partial x$. Even if we assume only radial dependence to the electron density, there will be azimuthal variations to the moiré pattern because of the relationship $\partial n_e/\partial x = \cos(\theta)\partial n_e/\partial r$. Another difficulty is that absolute density measurements cannot be made in the closed hohlraum geometry. In previous measurements using moiré deflectometry [8] the density was obtained by integrating the measured density gradient along a path from some point of known density such as vacuum. Since the density gradient along the lip of the LEH cannot be determined, we can only obtain the relative density within the hohlraum. In order to gain useful electron density information we must consider the problem associated with both the cylindrical and closed geometry of the hohlraum.

First, we consider the complications of the cylindrical geometry. Using Eqs. (5), (7), and (8), we see that the moiré pattern is given by

$$T_M(x,y) = \cos\left(\frac{\pi}{p}\left\{y\,\theta + \frac{DL}{2n_c}\frac{\partial n_e}{\partial x}\right\}\right), \tag{12}$$

where we have approximated the integral in Eq. (8) by assuming the integrand is constant and L is the length of the hohlraum. Since the fringe pattern is formed by lines of constant phase, we can obtain a family of fringe curves by setting the total phase in Eq. (12) equal to $n\pi$, where $n = \pm 1, \pm 2, \ldots$. Therefore, the fringe pattern consists of curves given by

$$y = \frac{np}{\theta} - \frac{DL}{2\theta n_c}\frac{\partial n_e}{\partial x}. \tag{13}$$

Using Eq. (13) we can map out $\partial n_e/\partial x$ over the hohlraum. To find the complete gradient we also need $\partial n_e/\partial y$. This in principle can be done by rotating the hohlraum $\pi/2$ and repeating the experiment or by assuming radially symmetric density profiles.

Since the moiré fringes cannot be connected to the outside of the hohlraum, we can make an absolute density measurement only by assuming some density within the hohlraum. One possible solution is to take the image early in time before the blowoff plasma reaches the center of the hohlraum. The density at the center is either zero for empty hohlraums or some known value for gas filled hohlraums (assuming complete ionization of the gas). Even if we are unable to obtain absolute density measurements, relative density measurements will be valuable in understanding plasma blowoff and stagnation.

In order to demonstrate the utility of moiré deflectometry we show how a simple analysis of the smeared pattern of Fig. 7 gives reasonable estimates of the electron density. To avoid the complications of the $\cos(\theta)$ factor, we analyze the pattern near $y = 0$. In particular, we measure the fringe shifts around $y = 0.1$ and $x = 0.5$ mm. At this location we see about 1.8 fringe shifts over 200 μm. For the given values of D and p the sensitivity of our deflectometer is 0.26 mrad per fringe shift. Therefore, the moiré pattern at this point indicates 0.5 mrad over 200 μm. Using Eq. (8), we estimate the angular deflections to be $\delta\phi = \frac{1}{2}(n_e/n_c)(z/L)$, where z is the length of the plasma and L is the gradient scale length. Using $\delta\phi = 0.5$ mrad, $z = 1.0$ mm, and $L = 200$ μm, we find an electron density of about $n_e = 8.7\times10^{20}$. From the simulations we find the electron density to be around 6×10^{20} at this point and time.

V. CONCLUSIONS

Our calculations indicate that probing laser driven hohlraums appears quite feasible. The background emission is much lower than the collimated x-ray laser beam. We find that the signal-to-noise ratio is greater than 100. A ruling pitch (spacing) of $p = 10$ μm, grid rotation angle of $\theta = 2.5°$, and grid separation of 3.85 cm gives a fringe spacing and sensitivity to measure predicted angular deflections. With the appropriate timing and shortening (gating) of the x-ray laser pulse, temporal smearing of the moiré patterns is not a problem. Moiré deflectometry may be a valuable diagnostic tool for gaining information about the plasma density and stagnation.

[1] J. Lindl, Phys. Plasmas **2**, 3933 (1995).
[2] L. J. Suter, A. A. Hauer, L. V. Powers, D. B. Ress, N. Delameter, W. W. Hsing, O. L. Landen, A. R. Thiessen, and R. E. Turner, Phys. Rev. Lett. **73**, 2328 (1994).
[3] J. F. Seely, R. H. Dixon, R. C. Elton, and J. G. Lunney, J. Quant. Spectrosc. Radiat. Transf. **27**, 1297 (1982); C. De Michelis and M. Mattioli, Nucl. Fusion **21**, 677 (1981).
[4] R. P. Drake, D. W. Phillion, K. Estabrook, R. E. Turner, R. L. Kauffman, and E. M. Campell, Phys. Fluids B **1**, 1089 (1989).
[5] B. J. MacGowan, L. B. Da Silva, D. J. Fields, C. J. Keane, J. A. Koch, R. A. London, D. L. Matthews, S. Maxon, S. Mrowka, A. L. Osterheld, J. H. Scofield, G. Shimkaveg, J. E. Trebes, and R. S. Walling, Phys. Fluids B **4**, 2326 (1992), and references cited therein.
[6] O. Kafri and I. Glatt, *The Physics of Moiré Metrology* (Wiley, New York, 1990); K. Patorski, *The Moiré Fringe Technique* (Elsevier, New York, 1993).
[7] Lord Rayleigh, Philos. Mag. **47**, 193 (1874).
[8] D. Ress, L. B. Da Silva, R. A. London, J. E. Trebes, S. Mrowka, R. J. Procassini, T. W. Barbee, Jr., and D. E. Lehr, Science **265**, 514 (1994); L. Da Silva *et al.*, Bull. Am. Phys. Soc. **40**, 1748 (1995).
[9] J. Trebes *et al.*, Bull. Am. Phys. Soc. **40**, 1831 (1995).
[10] G. Zimmerman and W. Kruer, Comments Plasma Phys. Control. Fusion **11**, 51 (1975).
[11] D. Munro (private communication).
[12] David A. Liberman, J. R. Albritton, B. G. Wilson, and W. E. Alley, Phys. Rev. A **50**, 171 (1994).